AGU PUBLICATIONS

JGR

Journal of Geophysical Research: Atmospheres

RESEARCH ARTICLE
10.1002/2017JD027520

Key Points:
- Lightning EM fields are significantly affected by the presence of mountainous terrain
- The location errors of lightning location systems depend strongly on the used onset time estimation technique
- The elongated path method provides an effective real-time approach to improve the location errors of LLSs in mountainous regions

Location Accuracy Evaluation of ToA-Based Lightning Location Systems Over Mountainous Terrain

Dongshuai Li[1], Marcos Rubinstein[2], Farhad Rachidi[3], Gerhard Diendorfer[4], Wolfgang Schulz[4], and Gaopeng Lu[5,6]

[1]Climate Dynamics Research Center and Earth System Modeling Center, Nanjing University of Information Science and Technology, Nanjing, China, [2]Institute for Information and Communications Technologies, Yverdon-les-bains, Switzerland, [3]Electromagnetic Compatibility Laboratory, Swiss Federal Institute of Technology (EPFL), Lausanne, Switzerland, [4]OVE Service GmbH, Department ALDIS (Austrian Lightning Detection and Information System), Vienna, Austria, [5]Key Laboratory of Middle Atmosphere and Global Environment Observation, Institute of Atmospheric Physics, Chinese Academy of Sciences, Beijing, China, [6]Key Laboratory of Meteorological Disaster of Ministry of Education, Nanjing University of Information Science and Technology, Nanjing, China

Correspondence to:
D. Li,
dongshuaili@gmail.com

Citation:
Li, D., Rubinstein, M., Rachidi, F., Diendorfer, G., Schulz, W., & Lu, G. (2017). Location accuracy evaluation of ToA-based lightning location systems over mountainous terrain. *Journal of Geophysical Research: Atmospheres*, *122*, 11,760–11,775. https://doi.org/10.1002/2017JD027520

Received 27 JUL 2017
Accepted 11 OCT 2017
Accepted article online 18 OCT 2017
Published online 6 NOV 2017

Abstract In this paper, we analyze the location error of time of arrival (ToA)-based lightning location systems (LLSs) caused by propagation effects over mountainous terrain around the Säntis tower located in the Swiss Alps. The study is based on a full-wave three-dimensional (3-D) finite difference time domain approach using the topographic map including the Säntis tower and the nearby sensors belonging to LLSs. It is found that the vertical electric fields are strongly affected by the presence of the mountainous terrain and the finite ground conductivity and that the location error associated with the ToA technique depends strongly on the used onset time estimation technique. The evaluated location errors associated with amplitude thresholds of 10% and 20% and the time of the linear extrapolation of the tangent at maximum field derivative are found to be smallest (about 300 m or less). Finally, we assess the accuracy of two simplified methods (terrain envelope method and tight-terrain-fit method) to account for the location error due to propagation over mountainous terrain. These two methods might represent an efficient alternative to estimate the additional time delay due to propagation over a nonflat terrain by using available topographic data. In addition, a possible real-time location error compensation algorithm using the elongated propagation path method to improve the location error of the LLSs in mountainous regions is presented and discussed.

1. Introduction

The location accuracy of the time of arrival (ToA) technique used in lightning location systems (LLSs) is affected by propagation effects along a ground with finite conductivity (e.g., Cooray, 2009; Cooray et al., 2000; Delfino, Procopio, & Rossi, 2008; Delfino, Procopio, Rossi, Rachidi, et al., 2008; Rubinstein, 1996; Shoory et al., 2011) and/or rough and nonflat ground configurations (e.g., Cooray & Ming, 1994; Cummins et al., 2005; Last & Williams, 2000; Last et al., 2000; Li et al., 2013, 2014; Paknahad et al., 2014; Perez-Perez et al., 2013; Schulz & Diendorfer, 2000; Zhang, Yang, Jing, et al., 2012; Zhang, Yang, Li, et al., 2012). On one hand, several methods have been proposed to refine the algorithms for the estimation of the time of arrival associated with a measured waveform to minimize the propagation effects of the lossy ground (e.g., Cooray, 1987; Cummins et al., 2010; Honma et al., 2013, 1998; Liu et al., 2016; Schulz & Diendorfer, 2000; Schulz et al., 2016). On the other hand, propagation correction methods based on observation-based lightning data sets have been developed to improve the location accuracy of LLSs, such as in the U.S. National Lightning Detection Network (Cummins et al., 2010) and in the European Cooperation for Lightning Detection (EUCLID) network (Schulz & Diendorfer, 2000; Schulz et al., 2016). Recently, Paknahad et al. (2014) studied the propagation effects on lightning radiated electromagnetic fields by considering a pyramidal mountain and noted that the time delays and amplitudes of the lightning-radiated electromagnetic fields can be significantly affected by the mountainous terrain and associated diffraction phenomena. In another paper, Li, Rachidi, et al. (2016) further analyzed the location error of ToA-based LLSs by using a two-dimensional (2-D) finite difference time domain (FDTD) approach. To reduce the computational complexity, the axial symmetric assumption was made using 2-D topographic maps along the direct path between the lightning

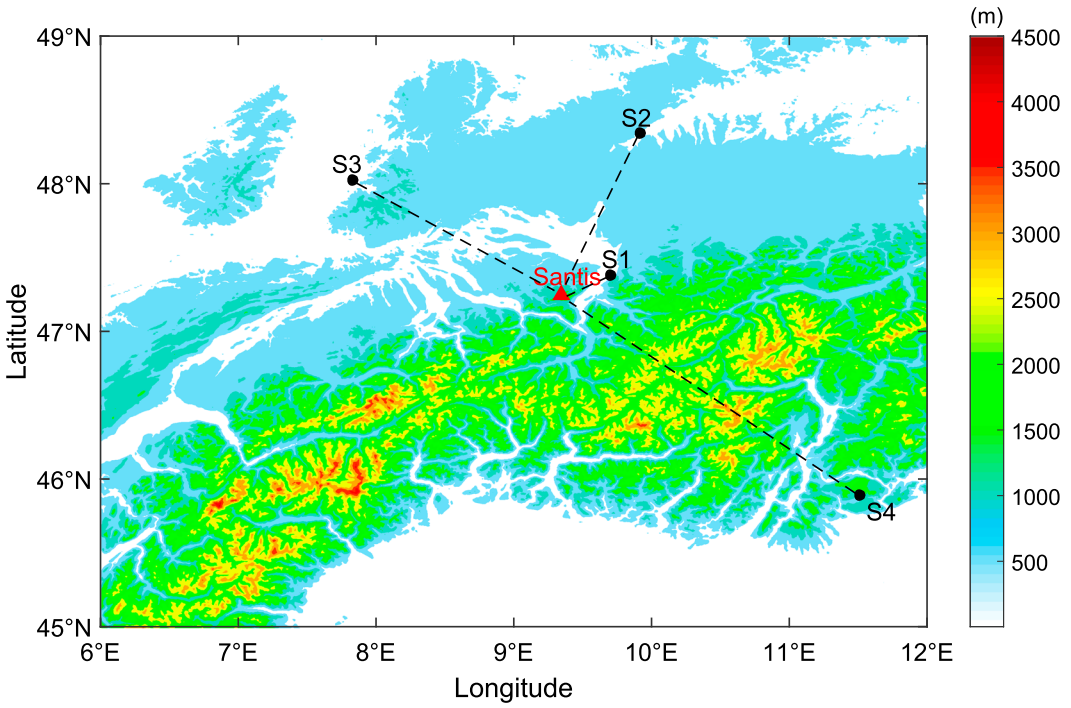

Figure 1. The topographic map of the selected region including the locations of four sensors (S1, S2, S3, and S4) in the region of the Säntis tower (red triangle).

location and nearby sensors. Their study showed that the location error strongly depends on the adopted threshold times.

In this paper, for the first time, the location accuracy of ToA-based LLSs over mountainous terrain is evaluated based on a three-dimensional (3-D) full-wave FDTD approach using available topographic data. The 3-D FDTD approach is used to analyze the propagation effects of the electromagnetic fields over mountainous terrain and to evaluate the location error associated with the ToA technique in LLSs. We also use the 3-D full-wave FDTD method to compare the accuracy of the calculated lightning locations corresponding to six different remote field onset time estimation methods. Then, the accuracy of two elongated propagation path methods (terrain envelope method) (Li, Azadifar, et al., 2016) and tight-terrain-fit method (Schulz & Diendorfer, 2000) is assessed to account for the location error resulting from the propagation over mountainous terrain. Finally, a possible real-time approach using any elongated path method to improve the accuracy of LLSs when propagation occurs over mountainous regions is discussed.

2. Adopted Models and Methods for the Analysis

2.1. Terrain Topography

In this study, we focus on the region around the Säntis tower (Romero et al., 2013) to assess the location error of ToA-based lightning location systems resulting from propagation over mountainous terrain. Figure 1 shows the topographic map of the selected region based on the global digital elevation model version 2 (GDEM V2) data from Advanced Spaceborne Thermal Emission and Reflection radiometer (ASTER) with a horizontal grid spacing of 1 arc sec (approximately 30 m). S1, S2, S3, and S4 are the locations of four sensors (black dots) belonging to the European Cooperation for Lightning Detection (EUCLID) network (Schulz et al., 2016). The red triangle marks the position of the Säntis tower, which is located on the top of Mount Säntis, in the northeastern part of Switzerland. The 124 m tall tower was instrumented for the measurement of lightning current waveforms and their time derivatives at two different heights (24 m and 82 m) along the tower. More details on the measurement sensors and instrumentation system can be found in Romero et al. (2012, 2013).

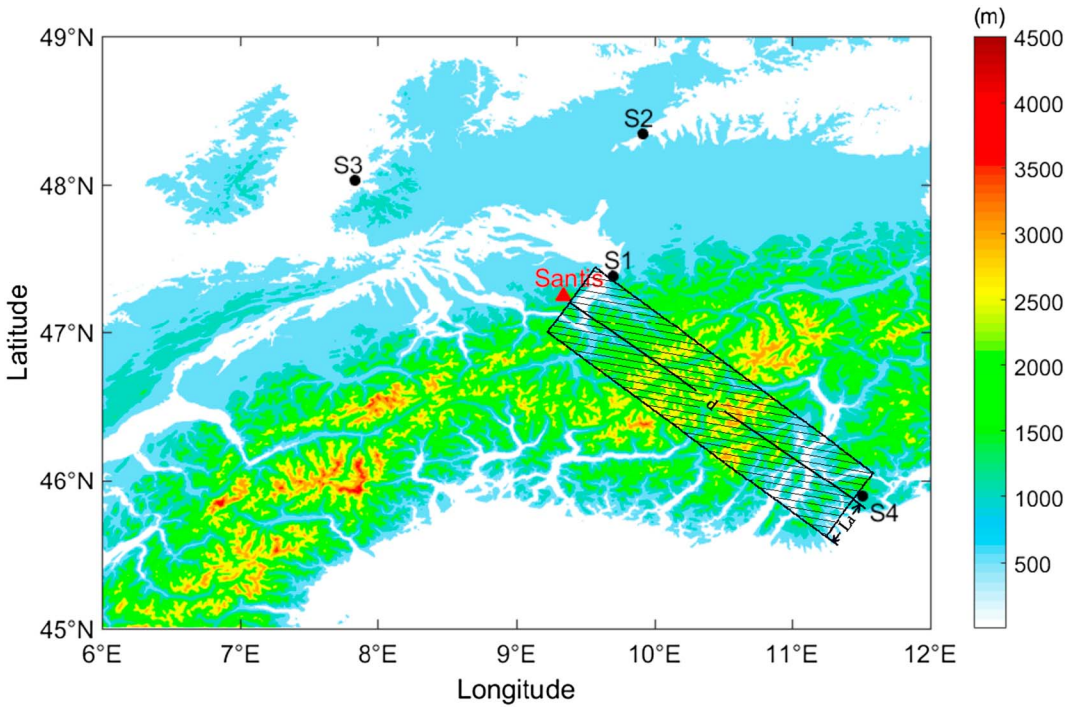

Figure 2. An example of the defined reference rectangular region for the 3-D FDTD model between the Säntis tower and the sensor site S4 with length d and width $L_d \times 2$ = 20 km.

2.2. FDTD Modeling

In order to take into account the topography between the Säntis tower and the nearby sensors, GDEM V2 data for the selected region (see Figure 1) are smoothed making use of the MATLAB Savitzky-Golay filter toolbox in order to remove all small-scale topographic fluctuation and interpolated to fit with the size of the spatial grid in the FDTD simulation (Li et al., 2015).

As discussed in Li et al. (2015), a three-dimensional (3-D) FDTD simulation of the full domain would require exorbitant computation time and memory consumption. On the other hand, the 2-D axial symmetric assumption might lead to inaccuracies. In this study, we have considered a reduced 3-D FDTD model of a rectangular area containing the region of interest. Figure 2 shows the rectangle considered for the propagation of electromagnetic fields from a lightning return stroke impacting on the Säntis tower to sensor S4. The width of the rectangle is $2 \times L_d$=20 km. Figures 3a, 3c, 3e, and 3g present the rectangular domains for each of the four considered sensors, S1, S2, S3, and S4. For comparison, Figures 3b, 3d, 3f, and 3h show the 2-D topographic profiles along the direct path between the Säntis tower and each sensor (Li, Rachidi, et al., 2016). The influence of the width L_d of the chosen reference region is analyzed in the appendix, where it is shown that considering a 20 km wide rectangular area results in an acceptable error level in the calculated field.

3. Analysis, Simulation Results, and Discussion

3.1. Calculation Parameters

For the FDTD analysis, the spatial discretization and the time increment were set to 50 m and 90 ns, respectively. The ground was considered as homogeneous with conductivity σ_g = 0.001 S/m. The value corresponds to conductivity measurements in the Alps (Marescot et al., 2008). The ground relative permittivity ε_{rg} is assumed to be equal to 10, which is commonly used in many studies. In the 3-D-FDTD analysis, we used 10 layers of convolutional perfectly matching layers (Roden & Gedney, 2000) as the absorbing boundary conditions. The current distribution along the return stroke channel was specified according to the modified transmission line model with exponential decay (Nucci et al., 1988; Rachidi & Nucci, 1990), assuming a current decay constant λ = 2 km (Nucci & Rachidi, 1989). The channel height was assumed to be H = 8 km, and the

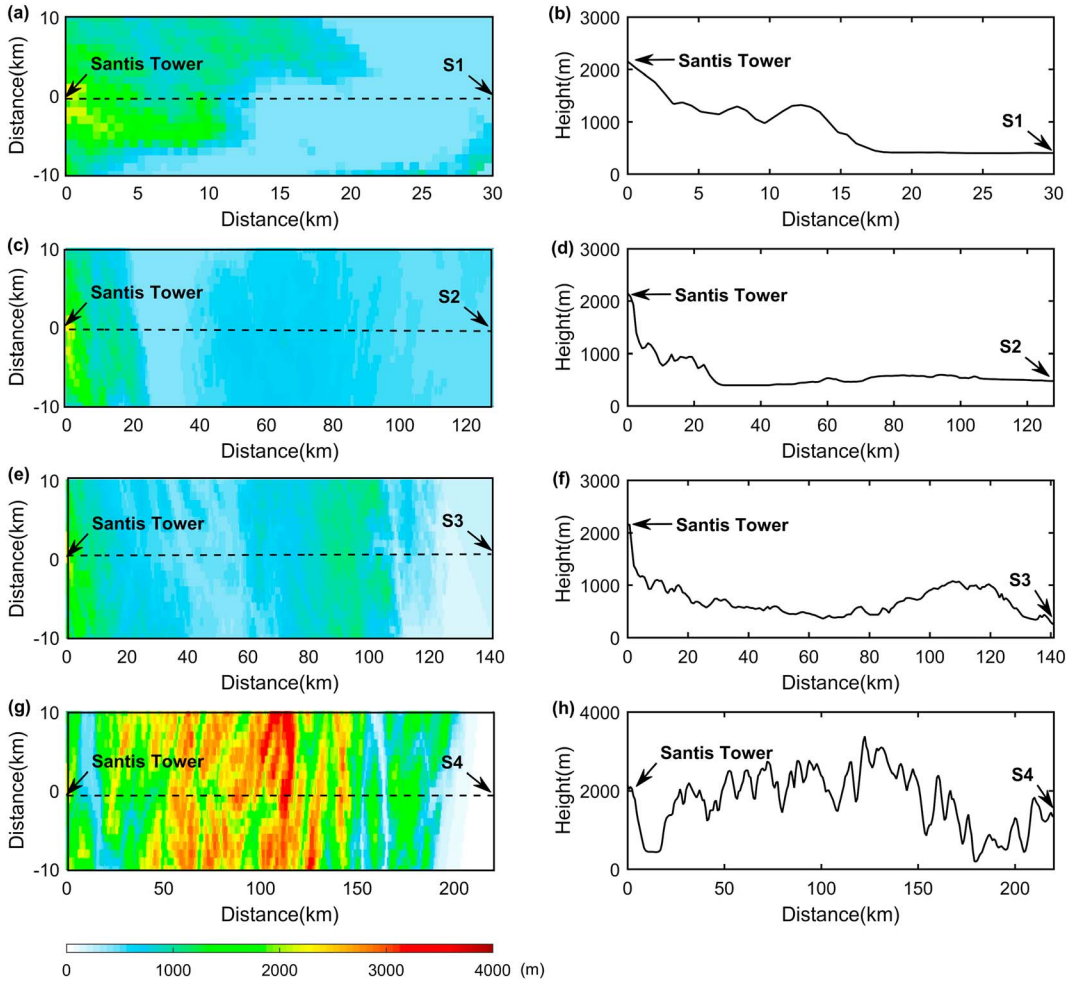

Figure 3. The (a, c, e, and g) reference region (left) and the (b, d, f, and g) 2-D cross section (right) of the topographic profiles along the direct path between the Säntis tower and the observation sensor site S1 (Figures 3a and 3b), S2 (Figures 3c and 3d), S3 (Figures 3e and 3f) and S4 (Figures 3g and 3h).

return stroke speed was set to $v = 1.5 \times 10^8$ m/s. The channel-base current was represented using the sum of two Heidler's functions (Heidler, 1985) corresponding to a typical subsequent return stroke (Rachidi et al., 2001). Figure 4 shows the waveforms of the subsequent return stroke current and its time derivative. The current is characterized by a peak value of 12 kA and a maximum time derivative of 40 kA/μs.

3.2. Simulation Results and Discussion

In this section, we adopt the following approach to evaluate the location accuracy of ToA-based LLSs over the mountainous region around the Säntis tower. First, we consider a return stroke to the Säntis tower and compute the generated electromagnetic fields at different positions corresponding to the sensor sites by using the full-wave FDTD method. Then, the numerical results are used to determine the location of the lightning discharge based on the ToA technique. Finally, the estimated locations are compared with the actual Säntis tower location.

3.2.1. The Electromagnetic Fields Over Mountainous Terrain

Figure 5 shows the vertical electric fields calculated by using our FDTD approach at the positions corresponding to the four LLS sensors (S1, S2, S3, and S4). The computations were performed considering different models for the ground: (i) perfectly conducting, flat ground (black line); (ii) finitely conducting, flat ground, σ_g = 0.001 S/m, ε_{rg} = 10 (blue line); (iii) finitely conducting ground (σ_g = 0.001 S/m, ε_{rg} = 10), taking into account the 3-D terrain profile using the topographic map, over a 20 km wide rectangular area (red line);

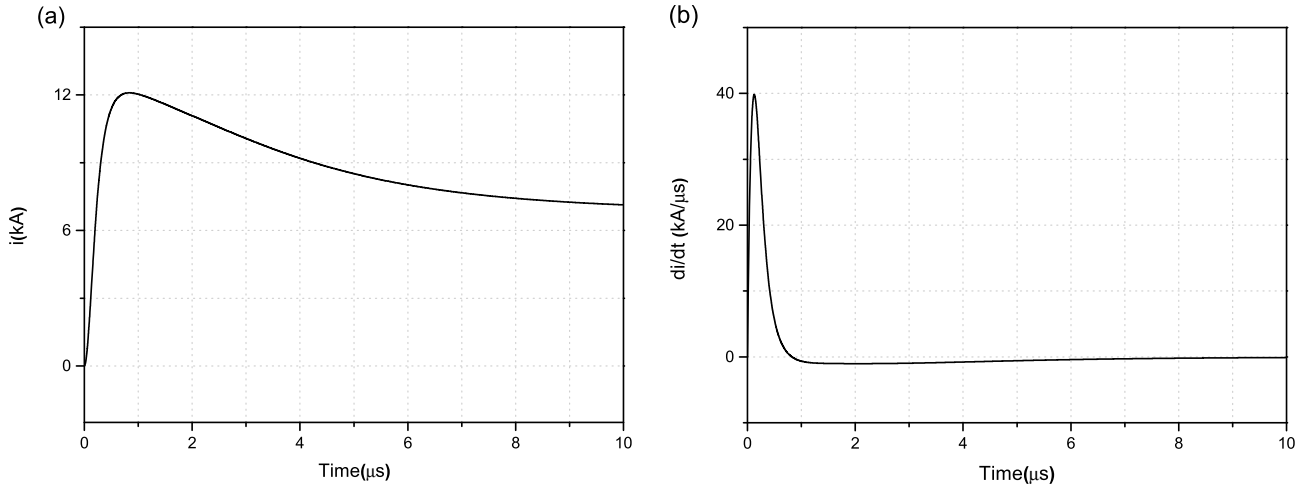

Figure 4. Subsequent return stroke current (a) waveform and (b) its time derivative waveform.

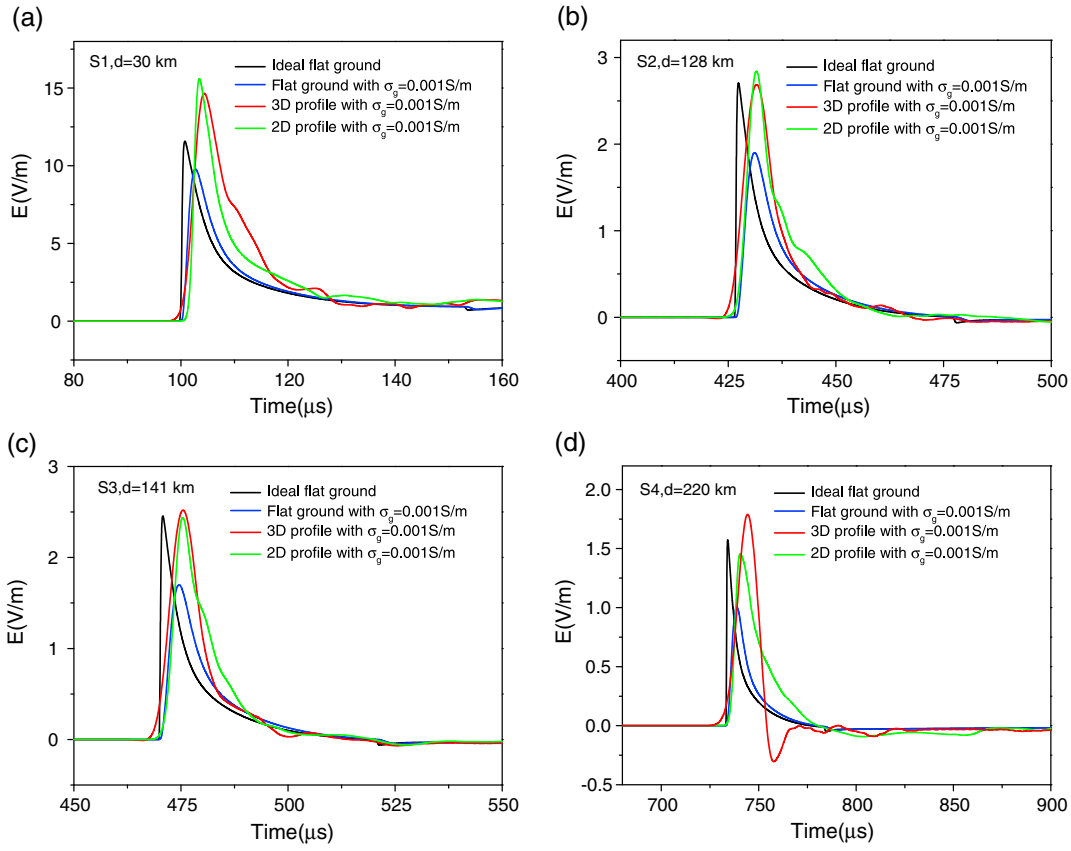

Figure 5. Vertical electric fields at each sensor ((a) S1, (b) S2, (c) S3, and (d) S4) considering different models for the ground. (i) Perfectly conducting, flat ground (black line); (ii) finitely conducting, flat ground, σ_g = 0.001 S/m, ε_{rg} = 10 (blue line); (iii) finitely conducting ground (σ_g = 0.001 S/m, ε_{rg} = 10), taking into account the 3-D terrain profile using the topographic map, over a 20 km wide rectangular area (red line); and (iv) finitely conducting ground (σ_g = 0.001 S/m, ε_{rg} = 10), taking into account the terrain profile using the 2-D topographic map along the direct path between the lightning location and each sensor (green line).

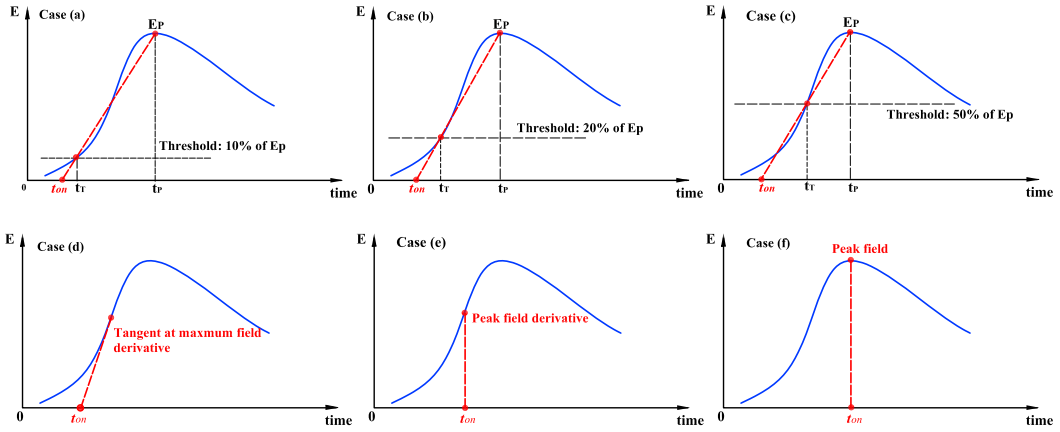

Figure 6. Calculation of the signal onset time ton associated with six different methods: (a) using an amplitude threshold of 10% of the initial rising amplitude of the field, (b) using an amplitude threshold of 20% of the initial rising amplitude of the field, (c) using an amplitude threshold of 50% of the initial rising amplitude of the field, (d) the zero-crossing time of the linear extrapolation of the maximum field derivative, (e) the time corresponding to the peak field derivative, and (f) the time corresponding to the peak field.

and (iv) finitely conducting ground (σ_g = 0.001 S/m, ε_{rg} = 10), taking into account the terrain profile along the 2-D topographic map along the direct path between the lightning location and each sensor (green line).

Note that cases (i)–(iii) are calculated using the 3-D FDTD method, while the results corresponding to case (iv) are computed by way of the 2-D FDTD approach presented by Li, Rachidi, et al. (2016).

From Figure 5, it can be seen that the vertical electric fields can be strongly affected by the presence of mountainous terrain and the finite ground conductivity. The assumption of a finitely conducting flat ground might result in a significant underestimation of the peak electric field (see blue and red lines in Figure 5), in agreement with the results presented by Li et al. (2015) and Azadifar et al. (2016). Note that as expected, after taking into account the propagation effect of the finite ground conductivity and the mountainous terrain, the rise times of the vertical electric fields in Figure 5 become longer.

It is interesting to note that the results obtained using the approximate 2-D approach (Li, Rachidi, et al., 2016) are very similar to those obtained using the 3-D FDTD method for the cases corresponding to sensors S1, S2, and S3. On the other hand, for sensor S4, the results obtained using the 2-D FDTD approach are significantly different from those obtained using the 3-D approach. This is due, on the one hand, to the fact that the propagation distance to sensor S4 is much longer than for the other sensors and, on the other hand, to the complex terrain profile along the path between the Säntis tower and that particular sensor site, as can be seen from Figures 3g and 3h.

3.2.2. Evaluated Location of the Lightning Discharge Based On the ToA Technique

Different methods have been proposed to determine the time of arrival of a measured signal used by the ToA technique (e.g., Lojou et al., 2011; Schulz, 1997). In this study, the so-called onset time is used to determine the time of arrival of a field pulse at a given sensor of a ToA-based LLS. Note that all the involved parameters for calculating the onset time will be extracted from the numerical results obtained using our full-wave FDTD approach. Figure 6 illustrates six different methods considered in this study to compute the onset time t_{on} used to evaluate the time of arrival of the field. Three of these methods are based on the following equation (Schulz, 1997):

$$t_{on} = t_p - \frac{t_p - t_T}{E_p - E_{th}} E_p, \tag{1}$$

where t_T is the threshold time at which the signal exceeds an amplitude threshold E_{th}, E_p is the peak amplitude of the field, and t_p is the time corresponding to the peak amplitude. The values for the threshold times considered here correspond to (a) 10% of the initial rising amplitude of the field, (b) 20% of the initial rising amplitude of the field, and (c) 50% of the initial rising amplitude of the field, (Cooray, 1987),

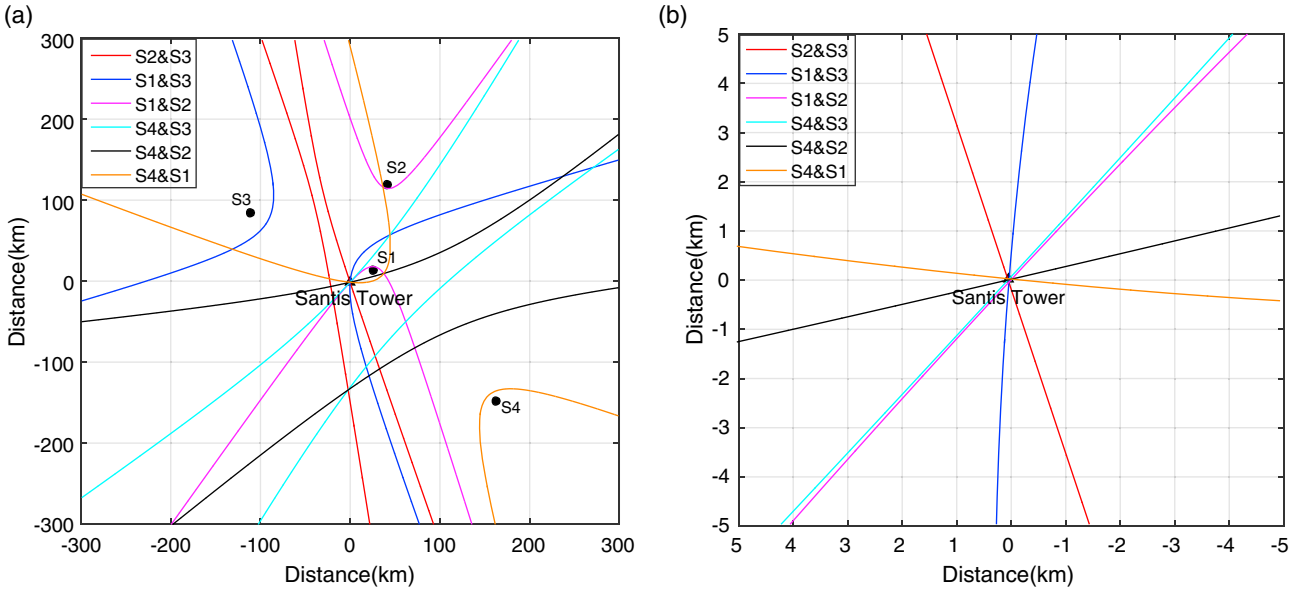

Figure 7. Lightning location results evaluated by the ToA technique for the ideal case of a flat, perfectly conducting ground using the FDTD approach. The presented areas are (a) 300 km × 300 km and (b) 5 km × 5 km, centered around the Säntis tower (triangle); six hyperbolas of different colors are shown corresponding to the following sensor pairs: S2-S3, S1-S3, S1-S2, S4-S3, S4-S2, and S4-S1.

The onset time is defined as the zero-crossing time of the straight line defined by the two points (t_p and E_p) and (t_T and E_{th}) (see cases a–c in Figure 6).

Additionally, three other methods were used to determine the onset time (see cases d–f in Figure 6), namely, (d) the zero-crossing time of the linear extrapolation of the tangent at maximum field derivative (Honma et al., 2013), (e) the time corresponding to the peak field derivative (Cooray, 1987), and (f) the time corresponding to the peak field.

Note that the improved linear extrapolation algorithm (case d) was used in the updated version of the EUCLID network from 2011, which was shown to have better accuracy compared to the previously used algorithms (Schulz et al., 2016).

Figure 7 gives the location results considering the ideal case of a flat, perfectly conducting ground. In the figure, pairs of hyperbolas associated with the differences in time of arrival between each pair of observation points (sensors) are shown. It is found that the ToA-predicted location coincides perfectly with the Säntis tower. Note that for the perfectly conducting flat ground case, the result is independent of the choice of the amplitude threshold in the determination of the onset time.

Figure 8 presents the plot of pairs of hyperbolas associated with the differences in time of arrival between each pair of observation points (sensors), in this case taking into account the 3-D terrain profile over a 20 km wide rectangular area and a finite conductivity of the ground (σ_g = 0.001 S/m and ε_{rg} = 10). It is found that the resulting hyperbolas strongly depend on the adopted onset time estimation technique, as can be seen by comparing to the perfectly conducting flat ground case in Figure 7. Note that after considering the effect of the terrain profile, the ToA hyperbolic branches do not exhibit a unique intersection point (see Figure 8). The estimate of the lightning strike position is then obtained from the minimum total distance point (MTDP) (solid green circle in Figure 8) by calculating the optimal minimization of the iterative equation below:

$$\mathrm{MTDP}(x,y) = \arg\min \sum_{i=2}^{4} \left| \left| \ (t_i - t_1) - T_{i,1} \right| \right|, \tag{2}$$

where the first term within the summation, $(t_i - t_1)$ is the measured time difference between the measured arrival times to the ith sensor, t_i, and the time of arrival to sensor 1, t_1 (sensor 1 corresponding to the reference sensor where the signal arrives first). The second term within the summation in (equation (2)) is the calculated time

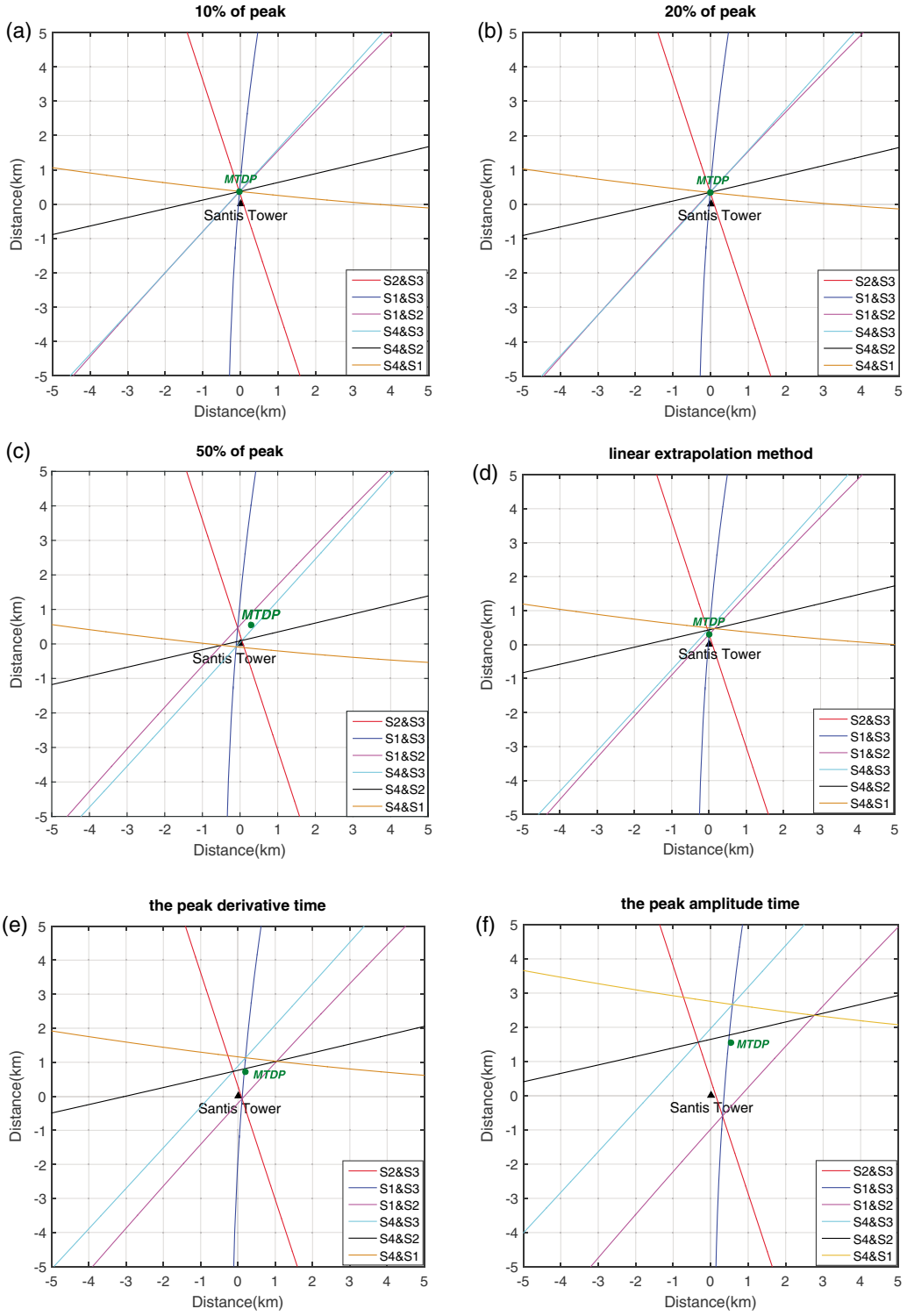

Figure 8. Lightning location results evaluated by the ToA technique taking into account the mountainous terrain and the finite conductivity of the ground (σ_g = 0.001 S/m and ε_{rg} = 10) associated with the six different approaches for the onset time: (a) using an amplitude threshold of 10% of the initial rising amplitude of the field, (b) using an amplitude threshold of 20% of the initial rising amplitude of the field, (c) using an amplitude threshold of 50% of the initial rising amplitude of the field, (d) the linear extrapolation of the maximum field derivative, (e) the peak field derivative time, and (f) the peak field time. The presented area is 5 km × 5 km, centered around the Säntis tower (triangle); the minimum total distance point (MTDP) is represented by a solid green circle; six hyperbolic branches of different colors are drawn corresponding to the hyperbolic branches for the following sensor pairs: S2-S3, S1-S3, S1-S2, S4-S3, S4-S2, and S4-S1.

Table 1
The Distance d Between MTDP and the Säntis Tower Position Corresponding to the Six Considered Onset Time Estimation Approaches

Different onset times	*d* (m)
Using an amplitude threshold of 10% of peak	356
Using an amplitude threshold of 20% of peak	343
Using an amplitude threshold of 50% of peak	624
The zero-crossing time of linear extrapolation of the tangent at maximum Field derivative	298
The time of peak field derivative	752
The time of peak field	1,651

difference $T_{i,1}=\sqrt{(X_i-x)^2+(Y_i-y)^2}/c-\sqrt{(X_1-x)^2+(Y_1-y)^2})/c$, where (x,y) is the prospective lightning source location, (X_i,Y_i) is the location of the ith sensor, (X_1,Y_1) corresponding to the reference sensor position, and c is the signal propagation velocity, which is assumed to be the speed of light. The iterative procedure is repeated by varying the values of x and y until the calculated MTDP converges to the optimal minimization of equation (2). Table 1 summarizes the distance d between MTDP and the Säntis tower position corresponding to the six different approaches of onset time estimation.

The evaluated location errors associated with amplitude thresholds of 10% and 20% of the peak and the time of the linear extrapolation of the tangent at maximum field derivative (Honma et al., 2013) are found to be smallest, about 300 m or less. On the other hand, the evaluated locations due to the time of the peak field derivative (Cooray, 1987) and the onset time using an amplitude threshold time of 50% of the peak (Cooray, 1987) appear to be more sensitive to the presence of mountainous terrain, resulting in relatively large location errors. The maximum evaluated location error found, d = 1651 m, corresponds to the case considering the time of the peak field.

4. Elongated Propagation Path Methods

In this section, we assess the accuracy of two simplified methods (terrain envelope method) (Li, Rachidi, et al., 2016) and tight-terrain-fit method (Schulz & Diendorfer, 2000) to account for the additional time delays resulting from the propagation over mountainous terrain. As explained in what follows, we apply the tight-terrain-fit method in a different manner compared to that used by Schulz and Diendorfer (2000).

There are two main differences between the algorithm of Schulz and Diendorfer (2000) and the one presented in this paper. The first one is related to the way the tight-terrain-fit method used. Schulz and Diendorfer (2000) proposed an iterative method in which each iteration in turn to estimate the possible location by calculating the tight-terrain-fit propagation delays to the sensors. The process continues until two successive iteration locations satisfy a predefined condition (such as a distance shorter than a given minimum). On the other hand, in the algorithm presented in this paper, the propagation delays from each sensor as a function of angle and distance are precalculated and the information is combined with the measured time of arrival times to determine the point for which the same stroke time is seen by each one of the sensors.

The second notable difference between the tight-terrain-fit method of Schulz and Diendorfer (2000) and the one presented in this paper is that the grid size used by Schulz and Diendorfer (2000) was adjusted to improve the obtained results, leading to an observed optimum for a large grid size of the order of a couple of kilometers by a couple of kilometers. Based on the results obtained in this paper, which we present below, we infer that the reason for Schulz and Diendorfer's observed grid size optimum is that, by using a large grid size, Schulz and Diendorfer (2000) were effectively averaging the main features of the terrain, inadvertently converting the tight-terrain-fit method to the terrain envelope method since the fine structure of the terrain was averaged out.

We will consider here the resulting location error corresponding to the speed-of-light propagation along the two elongated propagation paths and compare them with the results of the FDTD method. Figure 9 illustrates the two elongated propagation paths between the Säntis tower and each sensor (S1, S2, S3, and S4), namely, the terrain envelope method (blue line in Figure 9) and the tight-terrain-fit method (red line in Figure 9).

To evaluate the lightning location from the tight-terrain-fit method, we first calculated the distance from the Säntis tower to each one of the sensors along the tight-terrain-fit path. This corresponds to the lengths of the red lines in Figures 9a–9d. Next, we calculated the propagation time to each sensor by dividing its distance by the speed of light. We then calculated the time differences to each pair of sensors by subtracting the corresponding calculated propagation times. Finally, these differences in time of arrival were used to obtain an estimate of the lightning position based on the ToA technique assuming a flat and perfectly conducting ground. The same procedure was followed for the terrain envelope method using the lengths of the blue lines in Figure 9 to calculate the propagation times. Note that the blue line

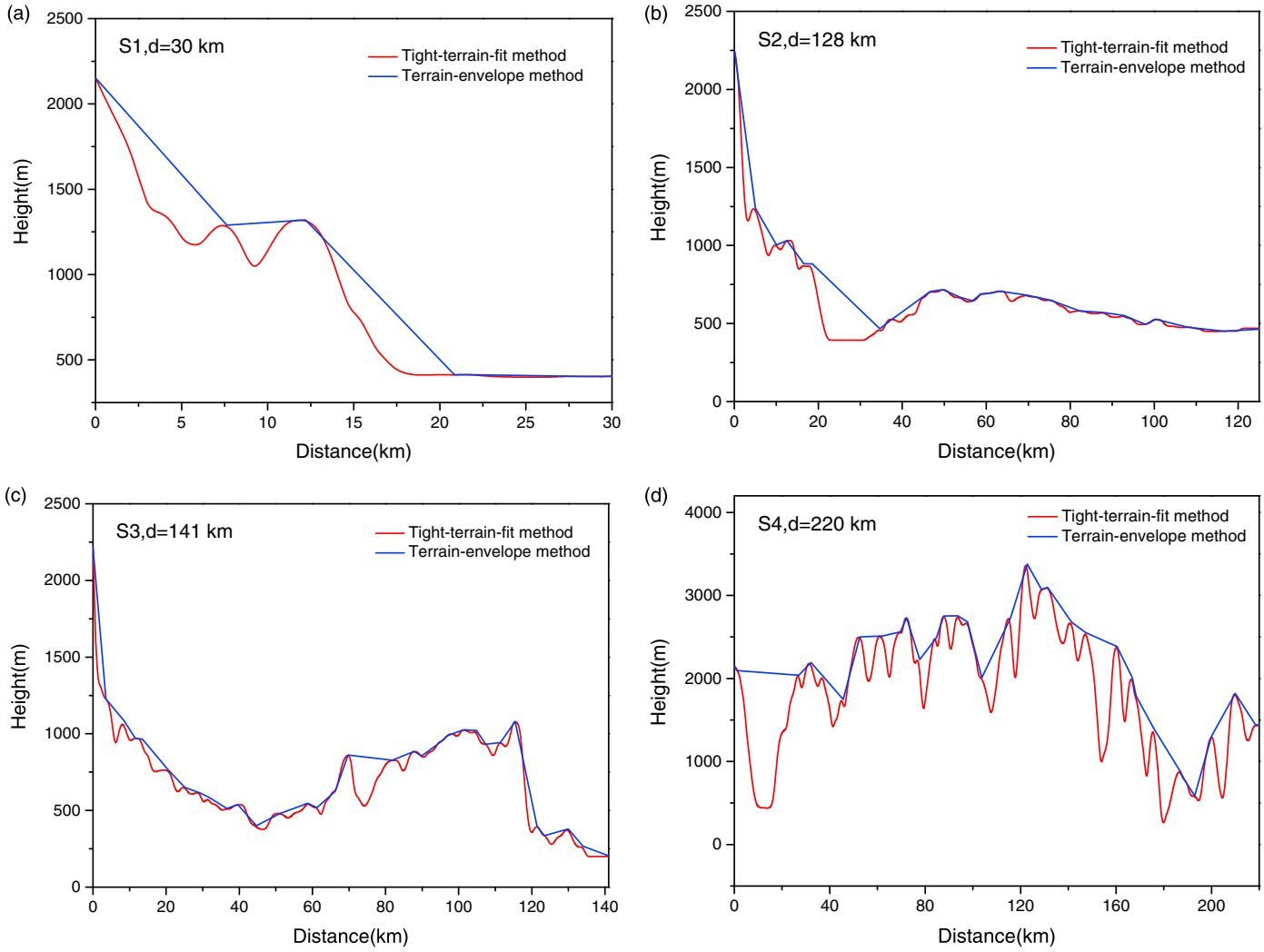

Figure 9. Illustration of two different elongated propagation path methods for the determination of the time delay of sensors (a) S1, (b) S2, (c) S3, and (d) S4, the terrain envelope method (blue line) and tight-terrain-fit method (red line).

corresponding to the terrain envelope method is the smallest convex polygonal chain, which was calculated in this paper using convhull, which is a MATLAB Convex Hull algorithm function, to obtain the terrain envelope path.

Figure 10 presents the results for the location following the procedure described in the previous paragraph, taking into account the terrain profiles based on the terrain envelope method and tight-terrain-fit method. For the considered configuration, the lightning location errors are also estimated by using the distance between the MTDP and the Säntis tower position, which are 1,998 m for the tight-terrain-fit method and 273 m for the terrain envelope method. For the considered case, it can be seen that the terrain envelope method is able to provide a better estimate of the location of the lightning strike (Säntis tower). It is interesting to note that the hyperbolas corresponding to the tight-terrain-fit method in Figure 10a are found to be very similar to those obtained with the FDTD numerical results considering the peak amplitude time shown in Figure 8f.

Taking as a reference a flat ground model, the extra length of the tight-terrain-fit method path and of the terrain envelope method path will appear as an additional time delay. Figure 11 further shows the additional time delays for each sensor corresponding to the speed-of-light propagation along the two elongated paths (tight-terrain-fit method and terrain envelope method) and those of the FDTD numerical approach considering the six different values of the onset time. The figure shows that the additional time delays introduced by

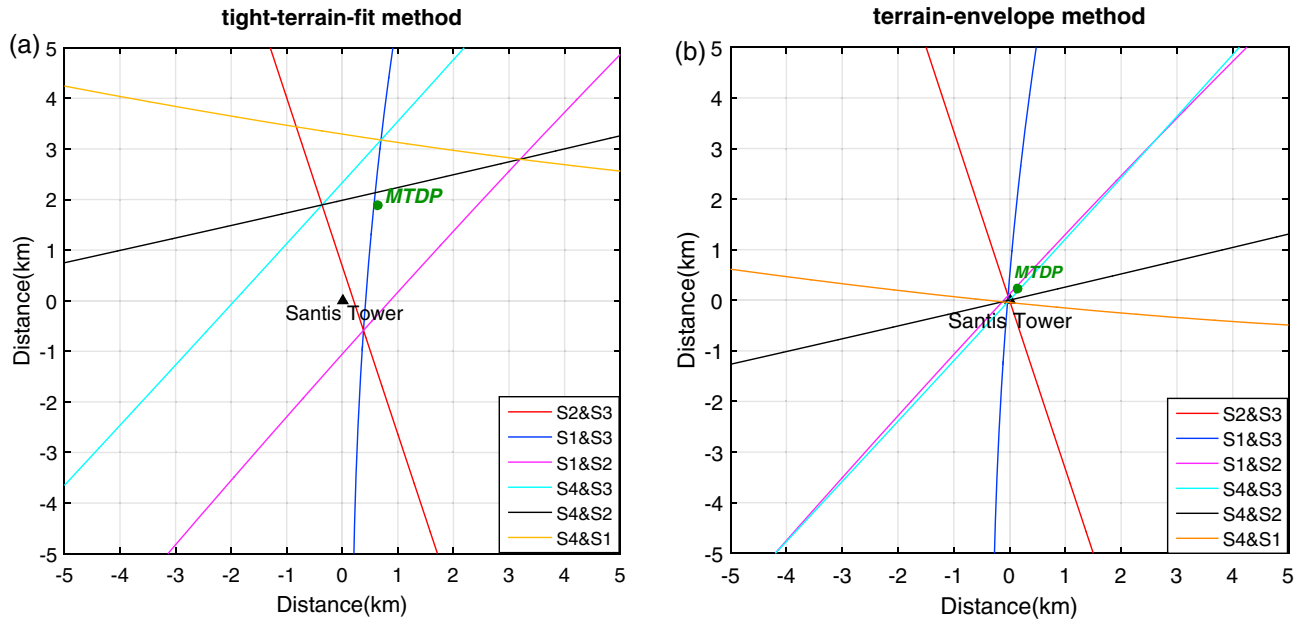

Figure 10. Hyperbolic branches calculated using the ToA technique for times of arrival calculated according to the two different elongated propagation path methods. (a) The tight-terrain-fit method and (b) the terrain envelope method. The presented area is 5 km × 5 km, centered around the Säntis tower (triangle), and the minimum total distance point (MTDP) is represented by a solid green circle.

the terrain envelope method agree well with the results obtained from our full-wave FDTD approach considering the time of the linear extrapolation of the maximum field derivative, an amplitude threshold of 10%, and an amplitude threshold of 20% of the initial rising amplitude of the field. On the other hand, the additional time delays calculated by using the tight-terrain-fit method are close to the FDTD results considering the time of peak.

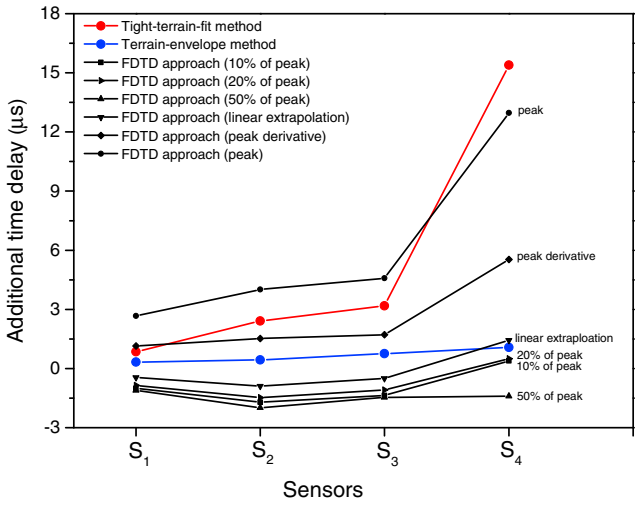

Figure 11. Additional time delays with respect to a flat ground for sensor sites S1, S2, S3, and S4 corresponding to the FDTD approach with the six different values of the onset time: (1) using an amplitude threshold of 10% of the initial rising amplitude of the field, (2) using an amplitude threshold of 20% of the initial rising amplitude of the field, (3) using an amplitude threshold of 50% of the initial rising amplitude of the field, (4) the time of the linear extrapolation of the maximum field derivative, (5) the peak field derivative time, and (6) the peak field time. Tight-terrain-fit method (red dots) and terrain envelope method (blue dots).

Based on these observations, we propose an algorithm in section 5 that uses available topographic data to compensate the measured arrival times for the effect of the mountains, which in turn allows the use of the flat ground equations to improve the location accuracy of ToA-based lightning location systems. The use of the considered configuration does not constitute a rigorous proof for the hypothesis, and more exhaustive tests would need to be performed to arrive at general conclusions. However, comprehensive testing would require excessive computational and time resources, and we have therefore left them as future work.

5. Location Error Compensation Algorithm for Mountainous Terrain

A possible real-time approach using the elongated propagation path methods (tight-terrain-fit method and terrain envelope method) to improve the location accuracy of LLSs involving propagation over mountainous terrain is discussed in this section. Based on the analysis of section 4, the evaluated location of a lightning discharge corresponding to the terrain envelope method is in good agreement with the FDTD numerical results, which might represent an interesting alternative to estimate the additional time delay due to the propagation over a nonflat terrain by using available topographic data and to compensate for this extra delay to obtain a better estimate of the strike location. Figure 12 presents the terrain map (left) and the additional

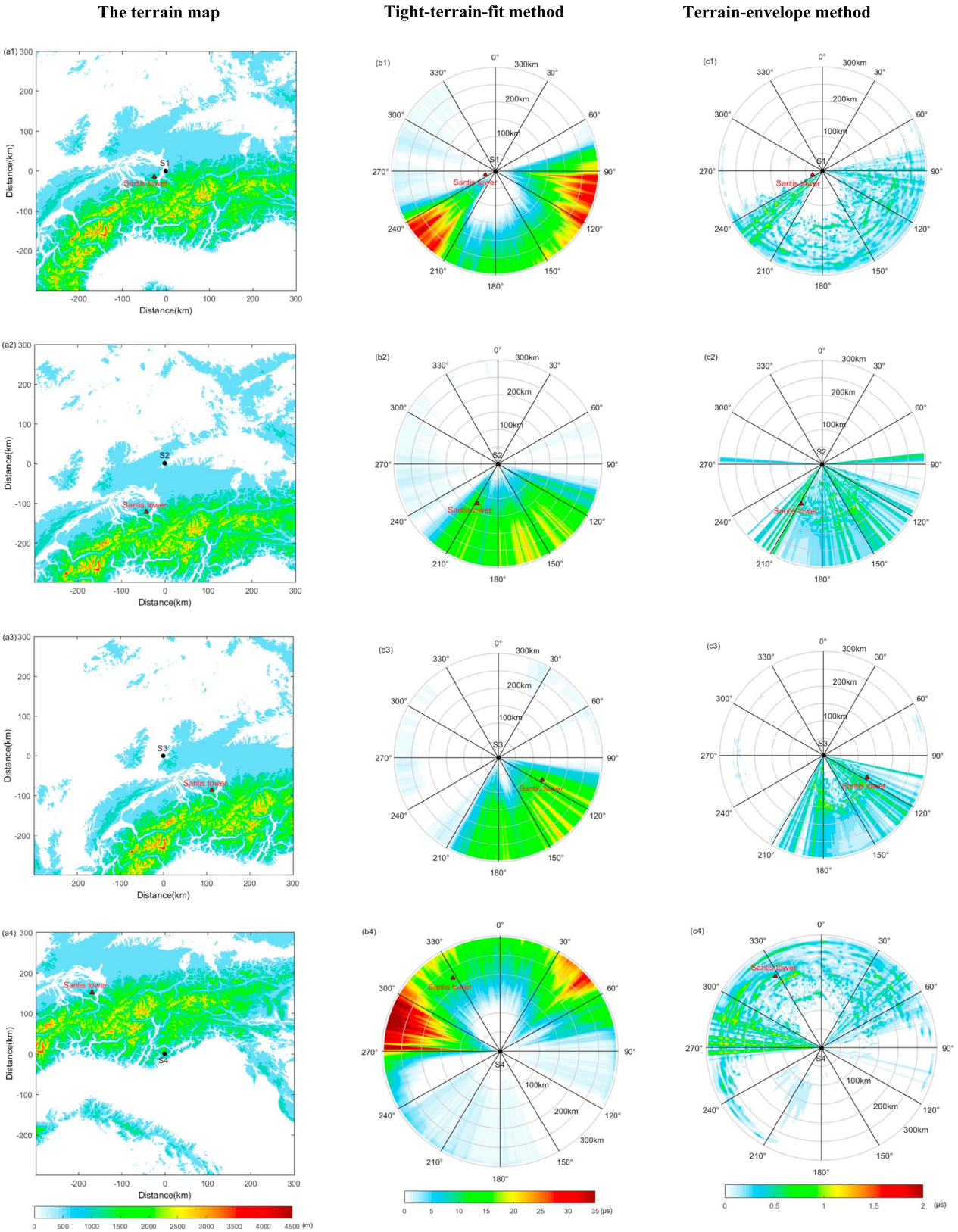

Figure 12. The (left column) terrain map and the additional time delay map centered around four sensors S1(a1,b1,c1), S2(a2,b2,c2), S3(a3,b3,c3) and S4 (a4,b4,c4) calculated by using the (middle column) tight-terrain-fit method and (right column) terrain envelope method. The presented area is 300 km × 300 km, the reference 0° direction is north, and the red triangle represents Säntis tower.

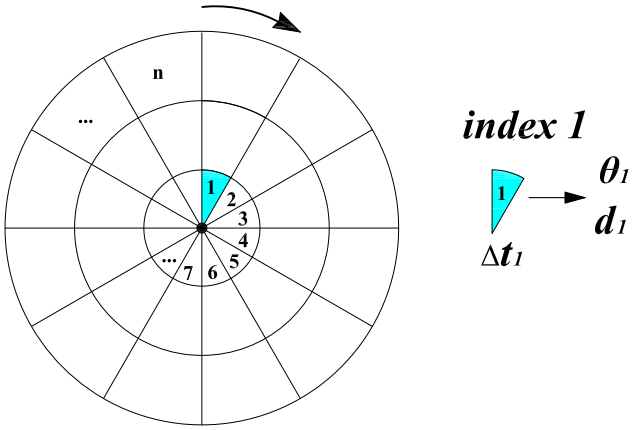

Figure 13. Indexes of different azimuth angle/distance pairs generated by following a clockwise spiral path. In the example, the indices *i* go from 1 to *n*. The black dot is the position of the centered sensor.

time delay map calculated by using the tight-terrain-fit method (middle) and terrain envelope method (right) with respect to the flat ground around the four sensors (S1, S2, S3, and S4) with different azimuth angles within a radius of 300 km. It can be seen that the additional time delays vary strongly as a function of the range and direction of propagation. This result is consistent with the study of Cummins et al. (2010). The tight-terrain-fit method, as expected, is more sensitive to the presence of mountainous terrain than the tight-envelop method.

If the extra time delay could be compensated for, the differences in time of arrival would correspond to those that would be measured if the ground were flat. Those compensated arrival times would therefore allow for a better estimation of the lightning strike point in real time. A possible real-time propagation correction using any elongated propagation path method to improve the location errors of the LLSs over mountainous region can be computed as follows, where steps 1 and 2 are carried out once, and the rest of the steps are followed for each detected stroke:

1. Define circular ring sectors around each sensor (black dot) as shown in Figure 13. Assign a unique identifier, which we will call index, as a function of distance d and azimuth angle θ, to each sector. In the figure, integers following a clockwise spiral path are used. Note that although a polar coordinate system, which has advantages in the areas close to the pole, is used here since it lends itself easily for the explanation of the technique, the algorithm can be readily modified to use with latitude and longitude as coordinates, which is preferable since, on the one hand, in the polar diagram the size of the sectors is sensitive to the distance d and, on the other hand, commercial systems use latitude and longitude. Note that in order to show the propagation characteristic clearly, we adopt a polar coordinate system in the example.
2. For each sensor i, create a five-column table as illustrated in Table 2. The first column identifies the sensor. The second column contains the identifying index of each circular ring sector. The third and fourth columns contain, respectively, the clockwise angle from the north to the axis of symmetry of the sector and the distance from the centered sensor (black dot in Figure 13) to the center of the sector. The fifth column contains the propagation time Δt_i from the center of the sector to the sensor location calculated using the elongated propagation path method. (Note that any method that produces accurate propagation times can, in principle, be used here, such as full-wave simulations or experimental data. However, the former would require prohibitively high computer resources and the latter is impractical and extremely costly.) This propagation time corresponds thus to a specific azimuth angle θ_i and distance d_i pair. Note that the choice of the granularity of the angles and distances will determine the maximum precision obtained with the algorithm.
3. For a given stroke detected by the LLS, obtain the arrival times T_i to each participating sensor.
4. Create new propagation times tables based on Table 2, changing the last column so that it contains $T_i - \Delta t_i$. This time corresponds to the stroke occurrence time since it is the time of arrival T_i minus the propagation time Δt_i.
5. Combine the tables of the participating sensors into a single global table.
6. Since the stroke time should be the same for all the sensors, the next step is to process the overall table to find the rows that contain the same stroke time (or similar stroke times since in practice the times will have some tolerance) in the last column. The search can be carried out as follows. First, sort the table in increasing stroke time order. Then, add a sixth column to the table in such a way that the sixth element of a row contains the difference between the strike time of that row and the strike time of the next row. The sixth cell of the last row can be left empty since it has no next row. Finally, select all the rows in which the new column contains a number smaller than a predefined tolerance. Any three consecutive rows satisfying that condition are a candidate to identify the angle and the distance from each participating sensor to the strike position.

Table 2
Propagation Times Table for Sensor i

Sensor	Index	Angle	Distance	Propagation times Δt
i	1	θ_1	d_1	Δt_1
i	2	θ_2	d_2	Δt_2
i	…	…	…	…
i	n	θ_n	d_n	Δt_n

Note. The number n correspond to individual angle and distance.

Note that the sorting of the stroke times in step 6 would be the most time consuming part in the algorithm. The sorting could be carried out in a tenth of a second on modern Laptops using for instance the radix sort algorithm.

It is worth noting that although the elongated propagation path method provides an interesting approach to improve the location errors of the LLSs when propagation occurs over mountainous terrain, for real-time use in practice, more studies involving other observation data (such as natural and rocket-triggered lightning) are needed.

6. Conclusions and Summary

In this paper, we analyzed the location error of time of arrival (ToA)-based lightning location systems (LLSs) due to propagation over mountainous regions. For the analysis, we considered the region around the Säntis tower in the Swiss Alps and the nearby sensor sites belonging to the EUCLID network. The analysis was based on a full-wave three-dimensional (3-D) finite difference time domain (FDTD) approach taking into account the terrain profile.

It was found that the vertical electric fields are strongly affected by the presence of mountainous terrain and the finite ground conductivity. We further evaluated the accuracy of six different approaches of onset time estimation used in the ToA technique by using our full-wave FDTD approach. It was shown that the location error associated with the ToA technique depends strongly on the adapted onset time calculation.

The evaluated location errors associated with amplitude thresholds of 10% and 20% and the time of the linear extrapolation of the tangent at maximum field derivative were found to be smallest, about 300 m or less. However, the evaluated locations derived using onset times based on the time of the peak field derivative and an amplitude threshold time of 50% of the peak appear to be more sensitive to the presence of mountainous terrain, resulting in relatively large location errors. The maximum evaluated location error is about 1,600 m, which is associated with the case considering the peak field time.

Finally, we assessed the accuracy of two simplified methods (terrain envelope method and tight-terrain-fit method) to account for the location error resulting from the propagation in a mountainous terrain. The preliminary analysis suggests that the terrain envelope method might represent an interesting alternative to estimate the additional time delay due to the propagation over a nonflat terrain by using available topographic data. In addition, a possible real-time location error compensation algorithm using any elongated propagation path method to improve the location errors of LLSs over mountainous region was presented and discussed.

Appendix A: The Effect of the Width of the Rectangular Area L_d

In this appendix, we discuss the influence of the adopted width of the reference rectangular area for our FDTD simulation. Figure A1 shows the vertical electric field calculated by using different widths (L_d) at

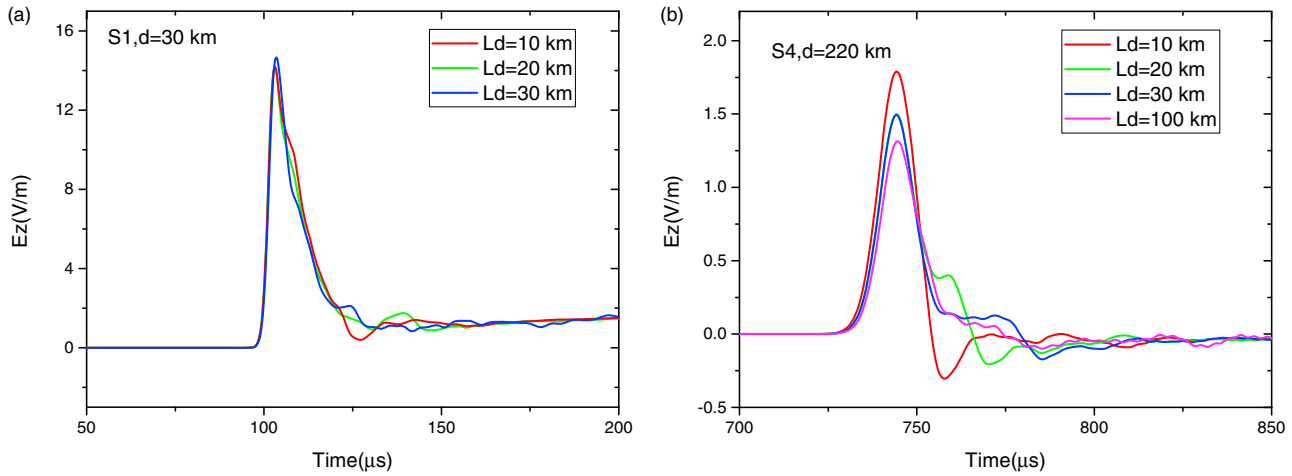

Figure A1. The effect of the width L_d of the reference area for the (a) S1 and (b) S4 sensor sites.

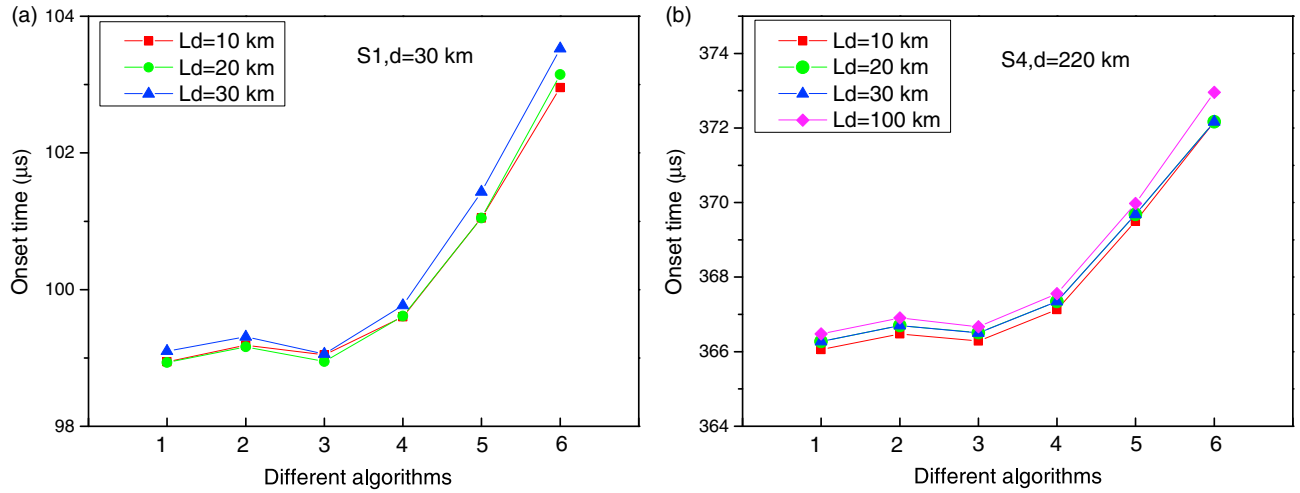

Figure A2. Onset times corresponding to six different algorithms for the (a) S1 and (b) S4 sensor sites. (1) using an amplitude threshold of 10% of the initial rising amplitude of the field, (2) using an amplitude threshold of 20% of the initial rising amplitude of the field, (3) using an amplitude threshold of 50% of the initial rising amplitude of the field, (4) the zero-corresponding time of the linear extrapolation of the maximum field derivative, (5) the peak field derivative time, and (6) the peak field time.

sensors S1 (d = 30 km) and S4 (d = 220 km). As can be seen, the numerical results at S1 sensor (close distance) are nearly insensitive when L_d varies between 10 and 30 km (see Figure A1). On the other hand, for farther distances (sensor S4), a difference of up to 20% is observed in the amplitude of the field when L_d varies from 20 km to 100 km. Figure A2 further gives the onset times calculated by using the six different methods defined in section 3.2.2 for sensors S1 and S4. It is found that all the onset times used by the ToA technique depend only on the initial rising front of the measured signal, which is not significantly affected by the considered width L_d. Therefore, in our case, the adopted width of L_d = 20 km appears to be reasonable.

Acknowledgments

This work was supported jointly by the Swiss National Science Foundation under project 200021_147058, National Key Basic Research and Development Program (2014CB441405), National Natural Science Foundation of China (41574179), Open Research Program of Key Laboratory of Meteorological Disaster (Nanjing University of Information Science and Technology) of Ministry of Education (KLME1414), "The Hundred Talents Program" of Chinese Academy of Sciences (2013068). The Advanced Spaceborne Thermal Emission and Reflection Radiometer (ASTER) Global Digital Elevation Model Version 2 (GDEM V2) product is available at no charge for any user pursuant to an agreement between METI and NASA, which is available at https://asterweb.jpl.nasa.gov/gdem.asp. The data presented in this paper are available upon request from the corresponding author at dongshuaili@gmail.com.

References

Azadifar, M., Rachidi, F., Rubinstein, M., Paolone, M., Diendorfer, G., Pichler, H., … Romero, C. (2016). Evaluation of the performance characteristics of the European Lightning Detection Network EUCLID in the Alps region for upward negative flashes using direct measurements at the instrumented Säntis tower. *Journal of Geophysical Research: Atmospheres*, *121*, 595–606. https://doi.org/10.1002/2015JD024259

Cooray, V. (1987). Effects of propagation on the return stroke radiation fields. *Radio Science*, *22*(5), 757–768. https://doi.org/10.1029/RS022i005p00757

Cooray, V. (2009). Propagation effects due to finitely conducting ground on lightning-generated magnetic fields evaluated using Sommerfeld's integrals. *IEEE Transactions on Electromagnetic Compatibility*, *51*(3), 526–531. https://doi.org/10.1109/TEMC.2009.2019759

Cooray, V., Fernando, M., Sörensen, T., Götschl, T., & Pedersen, A. (2000). Propagation of lightning generated transient electromagnetic fields over finitely conducting ground. *Journal of Atmospheric and Solar-Terrestrial Physics*, *62*(7), 583–600. https://doi.org/10.1016/S1364-6826(00)00008-0

Cooray, V., & Ming, Y. (1994). Propagation effects on the lightning-generated electromagnetic fields for homogeneous and mixed sea-land paths. *Journal of Geophysical Research*, *99*(D5), 10,641–10,652. https://doi.org/10.1029/93JD03277

Cummins, K., Cramer, J., Brooks, W., & Krider, E. (2005). On the effect of land: Sea and other Earth surface discontinuities on LLS-inferred lightning parameters. Paper presented at VIII International Symposium on Lightning Protection, Sao Paulo, Brazil.

Cummins, K., Murphy, M., Cramer, J., Scheftic, W., Demetriades, N., & Nag, A. (2010). Location accuracy improvements using propagation corrections: A case study of the US National Lightning Detection Network. Paper presented at preprints, 21st International Lightning Detection Conference, Orlando, FL.

Delfino, F., Procopio, R., & Rossi, M. (2008). Lightning return stroke current radiation in presence of a conducting ground: 1. Theory and numerical evaluation of the electromagnetic fields. *Journal of Geophysical Research*, *113*, D05110. https://doi.org/10.1029/2007JD008553

Delfino, F., Procopio, R., Rossi, M., Rachidi, F., & Nucci, C. A. (2008). Lightning return stroke current radiation in presence of a conducting ground: 2. Validity assessment of simplified approaches. *Journal of Geophysical Research*, *113*, D05111. https://doi.org/10.1029/2007JD008567

Heidler, F. (1985). Traveling current source model for LEMP calculation. Paper presented at Proc. 6th Int. Zurich Symp. Electromagn. Compat, Zurich, Switzerland.

Honma, N., Cummins, K. L., Murphy, M. J., Pifer, A. E., & Rogers, T. (2013). Improved lightning locations in the Tohoku region of Japan using propagation and waveform onset corrections. *IEEE Transactions on Power and Energy*, *133*(2), 195–202. https://doi.org/10.1541/ieejpes.133.195

Honma, N., Suzuki, F., Miyake, Y., Ishii, M., & Hidayat, S. (1998). Propagation effect on field waveforms in relation to time-of-arrival technique in lightning location. *Journal of Geophysical Research*, *103*(D12), 14,141–14,145. https://doi.org/10.1029/97JD02625

Last, D., William, P., & Dykstra, K. (2000). Propagation of Loran-C signals in irregular terrain-modelling and measurements: Part II; Measurements. Paper presented at 29th Annual Convention and Technical Symposium, International Loran Association, Washington, DC.

Last, D., & Williams, P. (2000). Propagation of Loran-C signals in irregular terrain-modelling and measurements: Part 1: Modelling. Paper presented at 29th Annual Convention and Technical Symposium, International Loran Association, Washington, DC.

Li, D., Azadifar, M., Rachidi, F., Rubinstein, M., Diendorfer, G., Sheshyekani, K., … Wang, Z. (2016). Analysis of lightning electromagnetic field propagation in mountainous terrain and its effects on ToA-based lightning location systems. *Journal of Geophysical Research: Atmospheres*, *121*, 895–911. https://doi.org/10.1002/2015JD024234

Li, D., Azadifar, M., Rachidi, F., Rubinstein, M., Paolone, M., Pavanello, D., … Wang, Z. (2015). On lightning electromagnetic field propagation along an irregular terrain. *IEEE Transactions on Electromagnetic Compatibility*, *58*(1), 161–171. https://doi.org/10.1109/TEMC.2015.2483018

Li, D., Rachidi, F., Rubinstein, M., Diendorfer, G., & Wang, Z. (2016). Location accuracy evaluation of ToA-based lightning location systems over mountainous terrain. Paper presented at 24th International Lightning Detection Conference (ILDC), San Diego, CA.

Li, D., Zhang, Q., Liu, T., & Wang, Z. (2013). Validation of the Cooray-Rubinstein (C-R) formula for a rough ground surface by using three-dimensional (3-D) FDTD. *Journal of Geophysical Research: Atmospheres*, *118*, 12,749–12,754. https://doi.org/10.1002/2013JD020078

Li, D., Zhang, Q., Wang, Z., & Liu, T. (2014). Computation of lightning horizontal field over the two-dimensional rough ground by using the three-dimensional FDTD. *IEEE Transactions on Electromagnetic Compatibility*, *56*(1), 143–148. https://doi.org/10.1109/TEMC.2013.2266479

Liu, Z., Koh, K. L., Mezentsev, A., Enno, S.-E., Sugier, J., & Füllekrug, M. (2016). Variable phase propagation velocity for long-range lightning location system. *Radio Science*, *51*, 1806–1815. https://doi.org/10.1002/2016RS006058

Lojou, J.-Y., Honma, N., Cummins, K. L., Said, R. K., & Hembury, N. (2011). Latest developments in global and total lightning detection. Paper presented at Lightning (APL), 2011 7th Asia-Pacific International Conference on, IEEE, Chengdu, China.

Marescot, L., Monnet, R., & Chapellier, D. (2008). Resistivity and induced polarization surveys for slope instability studies in the Swiss Alps. *Engineering Geology*, *98*(1–2), 18–28. https://doi.org/10.1016/j.enggeo.2008.01.010

Nucci, C. A., Mazzetti, C., Rachidi, F., & Ianoz, M. (1988). On lightning return stroke models for LEMP calculations. Paper presented at 19th International Conference on Lightning Protection, Graz, Austria.

Nucci, C. A., & Rachidi, F. (1989). Experimental validation of a modification to the transmission line model for LEMP calculation. Paper presented at 8th Symposium and Technical Exhibition on Electromagnetic Compatibility, Zurich, Switzerland.

Paknahad, J., Sheshyekani, K., Hamzeh, M., & Rachidi, F. (2014). Lightning electromagnetic fields and their induced voltages on overhead lines: The effect of a non-flat lossy ground. Paper presented at Lightning Protection (ICLP), 2014 International Conference, IEEE, Shanghai, China.

Perez-Perez, D. D. J., Herrera-Murcia, J. G., & Perez-Gonzalez, E. (2013). Experimental detection efficiency evaluation for a lightning location system on a mountainous region. Paper presented at Lightning Protection (XII SIPDA), 2013 International Symposium on, IEEE, Belo Horizonte, Brazil.

Rachidi, F., Janischewskyj, W., Hussein, A. M., Nucci, C. A., Guerrieri, S., Kordi, B., & Chang, J.-S. (2001). Current and electromagnetic field associated with lightning-return strokes to tall towers. *IEEE Transactions on Electromagnetic Compatibility*, *43*(3), 356–367. https://doi.org/10.1109/15.942607

Rachidi, F., & Nucci, C. (1990). On the Master, Uman, Lin, Standler and the modified transmission line lightning return stroke current models. *Journal of Geophysical Research*, *95*(D12), 20,389–20,393. https://doi.org/10.1029/JD095iD12p20389

Roden, J. A., & Gedney, S. D. (2000). Convolutional PML (CPML): An efficient FDTD implementation of the CFS-PML for arbitrary media. *Microwave and Optical Technology Letters*, *27*(5), 334–339. https://doi.org/10.1002/1098-2760(20001205)27:5%3C334::AID-MOP14%3E3.0.CO;2-A

Romero, C., Paolone, M., Rubinstein, M., Rachidi, F., Rubinstein, A., Diendorfer, G., … Zweiacker, P. (2012). A system for the measurements of lightning currents at the Säntis tower. *Electric Power Systems Research*, *82*(1), 34–43. https://doi.org/10.1016/j.epsr.2011.08.011

Romero, C., Rachidi, F., Paolone, M., & Rubinstein, M. (2013). Statistical distributions of lightning currents associated with upward negative flashes based on the data collected at the Säntis (EMC) tower in 2010 and 2011. *IEEE Transactions on Power Delivery*, *28*(3), 1804–1812. https://doi.org/10.1109/TPWRD.2013.2254727

Rubinstein, M. (1996). An approximate formula for the calculation of the horizontal electric field from lightning at close, intermediate, and long range. *IEEE Transactions on Electromagnetic Compatibility*, *38*(3), 531–535. https://doi.org/10.1109/15.536087

Schulz, W. (1997). Performance evaluation of lightning location systems, PhD thesis, Technical University of Vienna, Vienna, Auatria.

Schulz, W., & Diendorfer, G. (2000). Evaluation of a lightning location algorithm using an elevation model. Paper presented at 25th International Conference on Lightning Protection (ICLP), Rhodos, Greece.

Schulz, W., Diendorfer, G., Pedeboy, S., & Poelman, D. R. (2016). The European lightning location system EUCLID—Part 1: Performance analysis and validation. *Natural Hazards and Earth System Sciences*, *16*(2), 595–605. https://doi.org/10.5194/nhess-16-595-2016

Shoory, A., Mimouni, A., Rachidi, F., Cooray, V., & Rubinstein, M. (2011). On the accuracy of approximate techniques for the evaluation of lightning electromagnetic fields along a mixed propagation path. *Radio Science*, *46*, RS2001. https://doi.org/10.1029/2010RS004480

Zhang, Q., Yang, J., Jing, X., Li, D., & Wang, Z. (2012). Propagation effect of a fractal rough ground boundary on the lightning-radiated vertical electric field. *Atmospheric Research*, *104–105*, 202–208. https://doi.org/10.1016/j.atmosres.2011.10.009

Zhang, Q., Yang, J., Li, D., & Wang, Z. (2012). Propagation effects of a fractal rough ocean surface on the vertical electric field generated by lightning return strokes. *Journal of Electrostatics*, *70*(1), 54–59. https://doi.org/10.1016/j.elstat.2011.10.003